A unique circular path of moving single bubble sonoluminescence in water*

Rasoul Sadighi-Bonabi[a)†], Mona Mirheydari[a)b)], Homa Ebrahimi[a)], Nastaran Rezaee[a)b)], and Lida Nikzad[c)]

[a)] *Department of Physics, Sharif University of Technology, Tehran* 11365-91, *Iran*

[b)] *Department of Physics, Islamic Azad University Central Tehran Branch, Tehran* 14676-86831, *Iran*

[c)] *Laser and Optics Research School, Tehran* 14676-86831, *Iran*

(Received 10 October 2010; revised manuscript received 26 December 2010)

Based on a quasi-adiabatic model, the parameters of the bubble interior for a moving single bubble sonoluminescence (m-SBSL) in water are calculated. By using a complete form of the hydrodynamic force, a unique circular path for the m-SBSL in water is obtained. The effect of the ambient pressure variation on the bubble trajectory is also investigated. It is concluded that as the ambient pressure increases, the bubble moves along a circular path with a larger radius and all bubble parameters, such as gas pressure, interior temperature and light intensity, increase. A comparison is made between the parameters of the moving bubble in water and those in N-methylformamide. With fluid viscosity increasing, the circular path changes into an elliptic form and the light intensity increases.

Keywords: sonoluminescence, bubble trajectory, fluid viscosity, bremsstrahlung

PACS: 43.35.Hl, 43.25.+y **DOI:** 10.1088/1674-1056/20/7/074302

1. Introduction

Sonoluminescence is the light emission resulting from the nonlinear oscillations of a gas-filled bubble. The most fascinating fact about this phenomenon is the conversion of the low-intensity sound energy to the energetic photons.[1] The light with a short pulse width is produced by the violent collapse of the bubble, which depends on the bubble oscillation.[2] Since the discovery of the sonoluminescence, various models have been presented to explain the light emission.[3,4] In the thermal radiation model, the spectral shapes are related to the bubble interior temperature and the light intensity is determined by the number of microscopic process.[5] Vuong *et al.*[6] showed that an adverse gradient in the sound speed produced by the heat transfer prevents the flow from gathering and making shock front. The dependence of the sonoluminescence on the bubble interior pressure and the bubble interior temperature was also discussed. It has been shown that as the bubble is cooled, the number of the flashes increases accompanied by small changes in the bubble radius.[7,8]

In Ref. [9], the existence of OH radicals in water was demonstrated and it was also verified that at low vapour pressure, such as in 85% sulfuric acid, the dominant reaction contributed to the continuous spectrum of the emitted light is the electron-neutral atom and the electron-ion bremsstrahlung recombination. The weak ionization theory and the bremsstrahlung mechanism were reported earlier for the stable-SBSL by An and Ying.[10] The experiments performed by Xu *et al.*[11] demonstrated that the noble gas plays a significant role in the line spectra of all kinds of emission models.

The other aspect in studying this phenomenon is the bubble trajectory, which is dependent on the variation of the hydrodynamic force and the fluid viscosity. Recently, the moving single bubble sonoluminescence (m-SBSL), which is mostly obtained in N-methylformamide, was studied. In the m-SBSL, the bubble cannot be trapped at the pressure antinodes, so the light is emitted from the non-stationary bubble. Following the equation introduced by Magnuted and Legendre[12] in studying the hydrodynamic force effect on the bubble, Toegel *et al.*[13] studied the bubble dynamics by using isothermal approach and identified that the history force is the origin of destabilization in the m-SBSL. In quasi-adiabatic compression assump-

*Project supported by the Research Deputy of Sharif University of technology, Iran.

†Corresponding author. E-mail: sadighi@sharif.ir

© 2011 Chinese Physical Society and IOP Publishing Ltd

tion, the bubble is heated up uniformly.[14] By using this model, Lofsted *et al.*[15] studied the variation of the bubble radius. The investigation on the unknown parameters of the sonoluminescence was performed by Barber *et al.*[16] Although in 2000, the m-SBSL was observed in water by Didenko *et al.*,[7] to the best of our knowledge, the bubble trajectory in this valuable host fluid has never been investigated.

In this work, for the first time, the bubble trajectory in water is calculated. The ambient pressure, at which all bubble parameters are maximized for the m-SBSL, is identified. It is found that the bubble moves along a complete circular path and turns into an elliptic one with the increase of the viscosity in the presence of other viscous host fluid, such as N-methylformamide. Furthermore, the light intensity is calculated by this model according to the variations of the bubble interior temperature and the bubble interior gas pressure in water. It is also noticed that as the fluid viscosity increases, the emitted light becomes more intense.

2. Mathematical model

2.1. Radial and translational dynamics

Radial dynamics of the bubble is studied by using the Rayleigh–Plesset equation and the full expression of the hydrodynamic force governing the bubble translational motion. This is justified because the mass and the heat are not transferred in the very short collapse time. The adiabatic model is limited to the collapse time.[17,19]

In the study of the radial dynamics of the bubble, the Rayleigh–Plesset equation is used in the following form with the equations of the boundary conditions implied:[18]

$$\rho_l\left(R\ddot{R}+\frac{3}{2}\dot{R}^2\right) = [P_{\rm gas}-P_0-P(t)]-4\nu\frac{\dot{R}}{R} - 2\sigma\frac{1}{R}+\frac{R}{C}\frac{\mathrm{d}}{\mathrm{d}t}(P_{\rm gas}), \quad (1)$$

where ρ is the fluid density, R is the bubble radius, ν is the shear viscosity of the fluid and σ is the surface tension. The $P(t)$ is the acoustical pressure exerted on the bubble,

$$P(t) = P_{\rm a}\sin(\omega t)\mathrm{j}_0\left(\frac{\pi\,|x|}{R_{\rm fl}}\right) = -P_{\rm a}\sin(\omega t)\left(1-\frac{\pi^2\,|x|^2}{6R_{\rm fl}^2}\right),$$

where $R_{\rm fl}=3$ cm is known as the resonator radius, $|x|$ is the position of the bubble measured from the centre of the resonator,[13] j_0 is the first term of the Bessel function, $P_{\rm a}$ is the initial driving pressure. The $P_0=1.031$ atm is the ambient pressure. The $P_{\rm gas}$ is the gas pressure inside the bubble, which follows a Van der Waals type equation[18]

$$\dot{P}_{\rm gas}(R,t) = \frac{\mathrm{d}}{\mathrm{d}t}P_{\rm gas}[R(t)] = -\gamma(R,\dot{R},t)\frac{3R^2\dot{R}}{R^3-h^3}P_{\rm gas}, \quad (2)$$

where h is the Van der Waals hard core radius and equals to $R_0/8.86$. The γ is the polytrophic component, which demonstrates the possibility of isothermal or adiabatic behaviour of the bubble interior and also measures the ratio between the heat advection and the heat diffusion.[19] The bubble interior temperature is given by

$$\dot{T} = -[\gamma(R,\dot{R},t)-1]\frac{3R^2R}{R^3-h^3}T. \quad (3)$$

The complete expression of the hydrodynamic force is derived by Magnaudet and Legendre[12] as

$$\begin{aligned}\boldsymbol{F}(t) = {} & 4\pi\rho\nu R(t)\boldsymbol{U}(t) \\ & +\frac{2}{3}\pi\rho\left\{\frac{\mathrm{d}[R(t)^3\boldsymbol{U}(t)]}{\mathrm{d}t}+2R(t)^3\frac{\mathrm{d}\boldsymbol{U}(t)}{\mathrm{d}t}\right\} \\ & +8\pi\rho\nu\int_0^t\exp\left[9\int_\tau^t R(t')^{-2}\,\mathrm{d}t'\right] \\ & \times\mathrm{erf}\left[\sqrt{9\nu\int_\tau^t R(t')^{-2}\,\mathrm{d}t'}\right]\frac{\mathrm{d}[R(\tau)\boldsymbol{U}(\tau)]}{\mathrm{d}\tau}\,\mathrm{d}\tau, \quad (4)\end{aligned}$$

where $\boldsymbol{U}$ is the relative velocity between the bubble and the fluid. The rate of a flow disturbance is measured by the Reynolds numbers. As the bubble has a radial and a translational motion, two Reynolds numbers are introduced. The radial Reynolds number is $R_{\rm er}=R|\dot{R}|/\nu$, where $\dot{R}$ is the radial bubble velocity. The translational Reynolds number is $R_{\rm et}=R|\boldsymbol{U}|/\nu$. It should be noted that when both Reynolds numbers are small, the expression of the hydrodynamic force exerted on the bubble is similar to that given by Eq. (5). However, when one of them is large, the total force becomes

$$\begin{aligned}\boldsymbol{F}(t) = {} & 12\pi\rho\nu R(t)\boldsymbol{U}(t) \\ & +\frac{2}{3}\pi\rho\left\{\frac{\mathrm{d}[R(t)^3\boldsymbol{U}(t)]}{\mathrm{d}t}+2R(t)^3\frac{\mathrm{d}\boldsymbol{U}(t)}{\mathrm{d}t}\right\}. \quad (5)\end{aligned}$$

Toegel *et al.*[13] presented a modified form for the coupled dynamics of the bubble radial and translational

motion by introducing two switches

$$\theta_{\rm r} = \frac{1}{1+\left(\dfrac{R_{\rm er}}{R_{\rm er,crit}}\right)^4}, \quad \theta_{\rm t} = \frac{1}{1+\left(\dfrac{R_{\rm et}}{R_{\rm et,Crit}}\right)^4},$$

with $R_{\rm er,crit} = 7.0$ and $R_{\rm et,crit} = 0.5$. According to Toegel's equation, the final translational equation is as follows:

$$\begin{aligned} R(t)^2\ddot{\boldsymbol{v}} = {} & \frac{\rm d}{{\rm d}t}[(18\nu R + 3R^2\ddot{R})(\boldsymbol{u}-\boldsymbol{v}) + 3R^3\dot{\boldsymbol{u}} - 2R^3\boldsymbol{g}] \\ & - 3R^2\dot{R}\dot{\boldsymbol{v}}3v\frac{\theta_{\rm r}\theta_{\rm t}}{R^2}[(6\nu R + 3R^2\ddot{R}) \\ & \times(\boldsymbol{u}-\boldsymbol{v}) + 3R^3\dot{\boldsymbol{v}}]. \end{aligned} \tag{6}$$

2.2. Light emission

In the model presented by Yasui,[14] all effects of the thermal conduction between the bubble and the fluid and the condensation of the water vapour, which is the result of the chemical reactions at the bubble wall, are taken into consideration. While the temperature of the bubble interior ranges from 10000 K to 20000 K, the spectrum of the light emission detected from the noble gas seems to be continuous and can be produced by the radiative recombination of the electrons and ions.[20] The final equation, which represents the light emission intensity of the bubble, is

$$I = (r_{\rm r}\overline{hf} + P_{\rm br,ion} + P_{\rm br,atom})r_{\rm e},$$

where, $r_{\rm r}$ is the rate of the radiative recombination, $r_{\rm e}$ is the escape rate of electrons from the bubble and $\overline{hf}$ is the resulting mean energy of the photons.[14]

3. Numerical simulation

In this work, the coupled radial and translational motion of the bubble is simulated and the m-SBSL trajectories in water and in N-methylformamide are simulated. The pressure amplitudes are selected according to the phase diagrams presented in Ref. [21] and the domain presented for ambient pressure (1.3–1.5 atm) in Ref. [22]. In the work presented by Didenko *et al.*,[7] the line spectrum of the emitted light was shown for water at $P_{\rm a} = 1.4$ atm, however the trajectory of the moving bubble was not identified. Here the light emission of the bubble is also studied numerically and the bubble path is shown to be circular and periodic. All the calculations are conducted with the driving frequency equal to 33.4 kHz according to Ref. [21], and the physical properties of water at $T = 23$ °C are shown in Table 1 and compared with those of N-methylformamide.

Table 1. Physical properties of water and N-methylformamide at 23 °C.[23]

Fluid	C/m·s^{-1}	ρ/Kg·m^{-3}	$\nu/10^{-6}$ m^2·s^{-1}	σ/N·m^{-1}
Water	1485	998	–1	0.072
N-methylformamide	1660	1000	1.65	0.038

In Figs. 1–5, different characteristics of the sonoluminescing bubble, including dimensionless radius, bubble trajectory, bubble interior temperature, interior gas pressure and light intensity, are respectively compared for three pressure amplitudes in water. The three initial conditions are chosen as follows: $R_0 = 5$ μm, $P_{\rm a} = 1.36$ atm (1 atm = 1.01325×10^5 Pa); $R_0 = 6$ μm, $P_{\rm a} = 1.45$ atm; and $R_0 = 7$ μm, $P_{\rm a} = 1.5$ atm.

In Fig. 1, the variations of the bubble radius during one acoustical cycle for three different initial conditions are compared. The variation of the driving pressure is also plotted. We can see that these variations are in phase. During each acoustical cycle, in the first half of the cycle, as the driving pressure decreases, the bubble radius increases up to a maximum value. In the second half of the cycle, with driving pressure increasing, the bubble radius diminishes. The numerical calculation was performed for 20000 acoustical cycles and the scales are chosen to be dimensionless.

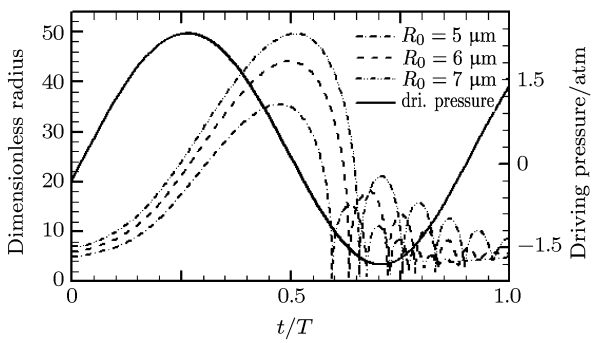


Fig. 1. The bubble radius and the driving pressure versus time during one cycle.

The trajectories of the bubble is drawn for the selected radii and the selected pressure amplitudes

(Fig. 2). It is shown that as the pressure amplitude and the initial radius increase, the bubble moves along a longer trajectory. Sadighi-Bonabi *et al.*[17] reported that the translational motion of the bubble starts near the centre of the resonator. In the present paper, the initial coordinate, $x_0 = 17$ μm, $y_0 = 7$ μm and $z_0 = 124$ μm, is selected precisely to identify the trajectory of the bubble.

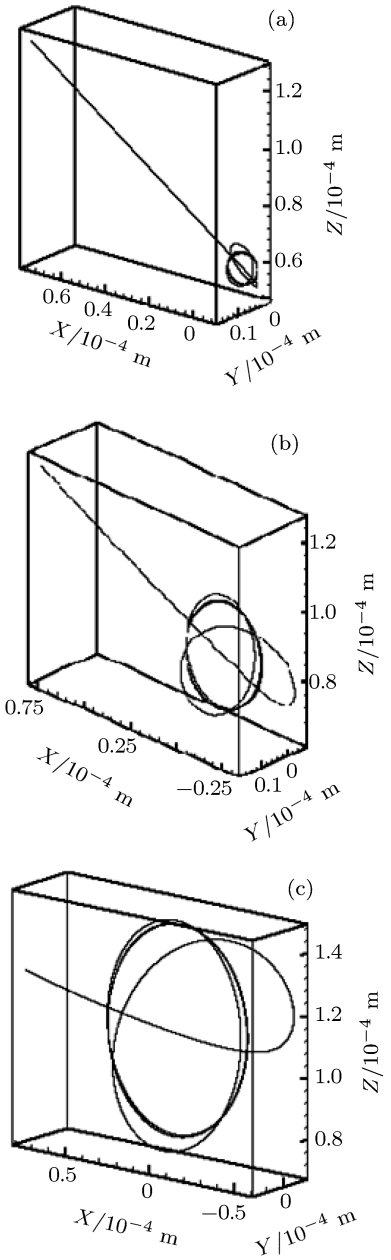


Fig. 2. The bubble trajectories in the cases of (a) $R_0 = 5$ μm and $P_a = 1.36$ atm, (b) $R_0 = 6$ μm and $P_a = 1.45$ atm and (c) $R_0 = 7$ μm and $P_a = 1.5$ atm.

Another parameter that affects the bubble intensity is the variation of temperature during the collapse and the expansion of the bubble. In Fig. 3, it is shown that as the pressure amplitude of the bubble increases, the bubble interior temperature increases and its variation is more distinctive. This also shows the dependence of the bubble temperature on its spatial position.

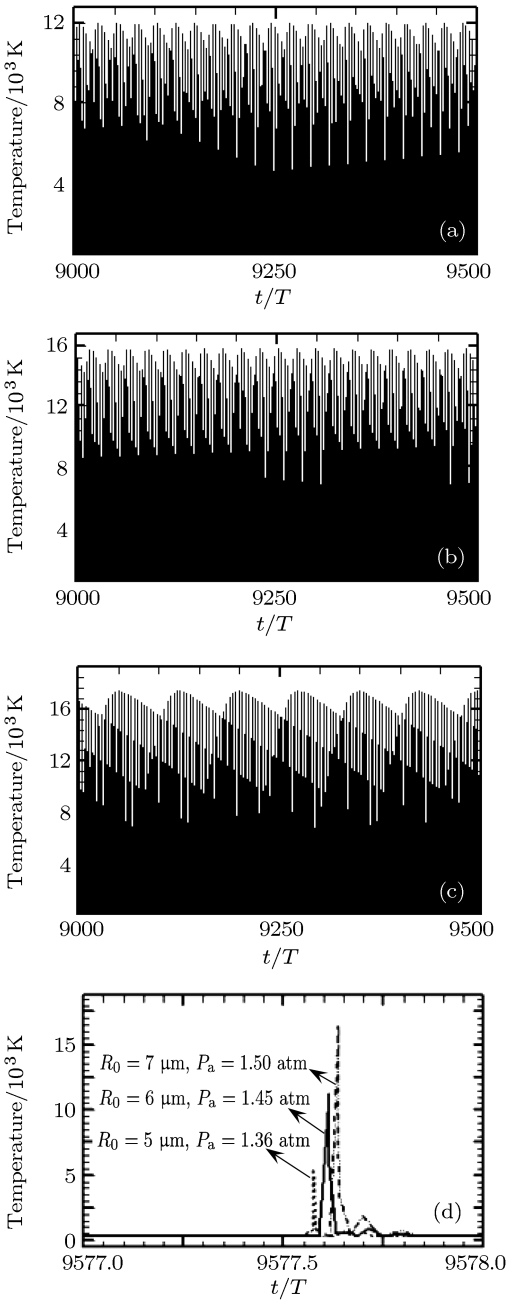


Fig. 3. The bubble interior temperature for the selected pressure amplitudes and the selected radii. The parameters are (a) $R_0 = 5$ μm, $P_a = 1.36$ atm, (b) $R_0 = 6$ μm, $P_a = 1.45$ atm and (c) $R_0 = 7$ μm, $P_a = 1.5$ atm. (d) A comparison among the maxima.

The interior gas pressure is shown in Fig. 4. During the bubble expansion, its volume increases enormously, so the interior gas pressure decreases correspondingly. During the bubble collapse, the applied pressure increases, accompanied by a reduction in the radius, thus the interior pressure increases.

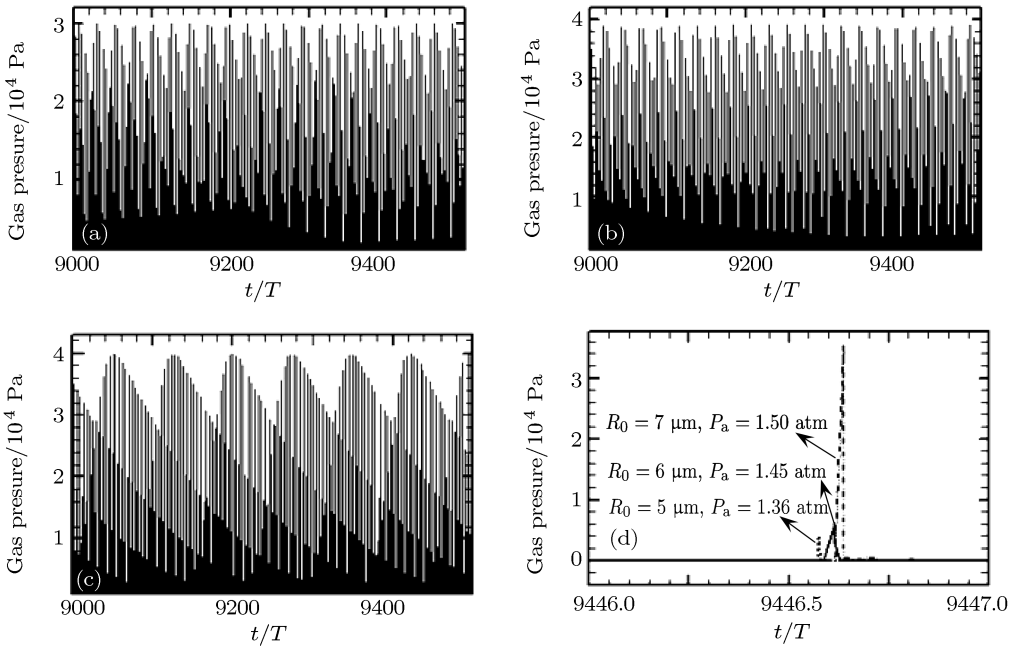


Fig. 4. The interior gas pressure versus time during 500 cycles. The parameters are (a) $R_0 = 5$ μm, $P_a = 1.36$ atm, (b) $R_0 = 6$ μm, $P_a = 1.45$ atm and (c) $R_0 = 7$ μm, $P_a = 1.5$ atm. (d) A comparison among the maxima.

At the moment of bubble collapse during each cycle, bright flashes of light are observed. According to the ambient conditions, the brightness for each flash is different. Figure 5 shows that with ambient pressure and initial radius increasing, the light intensity increases. In Fig. 5, it can also be observed that as the bubble interior temperature increases, the maximum of the light intensity increases. The light that appears at the moment of bubble collapse is proportional to the bubble interior temperature. The emission consists of short bright flashes, which result from the atomic and molecular excitation inside the bubble.

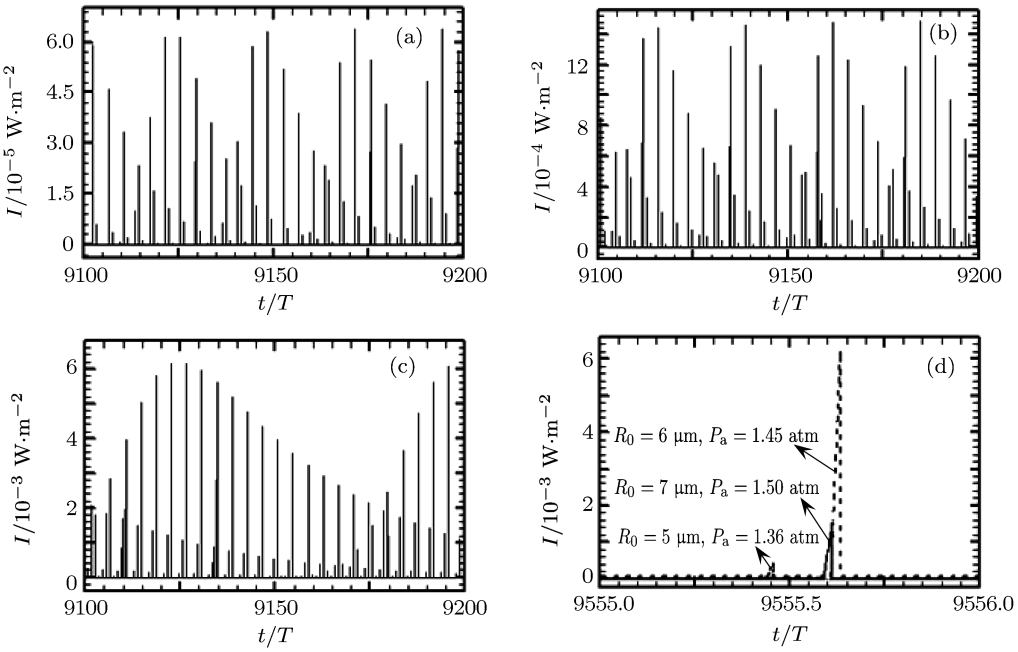


Fig. 5. Light intensities for the selected initial conditions: (a) $R_0 = 5$ μm, $P_a = 1.36$ atm, (b) $R_0 = 6$ μm, $P_a = 1.45$ atm, and (c) $R_0 = 7$ μm, $P_a = 1.5$ atm. (d) A comparison among the light intensities.

Figures 6–8 show the comparisons between the properties in water and in N-methylformamide for the selected pressures and the selected relative radii. The initial conditions for the bubble in N-methylformamide are $R_0 = 8$ μm, $P_a = 1.56$ atm. According to the earlier experimental results reported by Didenko *et al.*,[7] the bubble parameters increases with the fluid viscosity increasing.

Sadighi-bonabi *et al.*[17] presented an optimum pressure, with which all bubble parameters were maximized. In the report by Didenko *et al.*,[7] the brightness of the light flashes resulting from N-methylformamide were compared with that from water, though here a comparison is made among bubble parameters at these selected pressures.

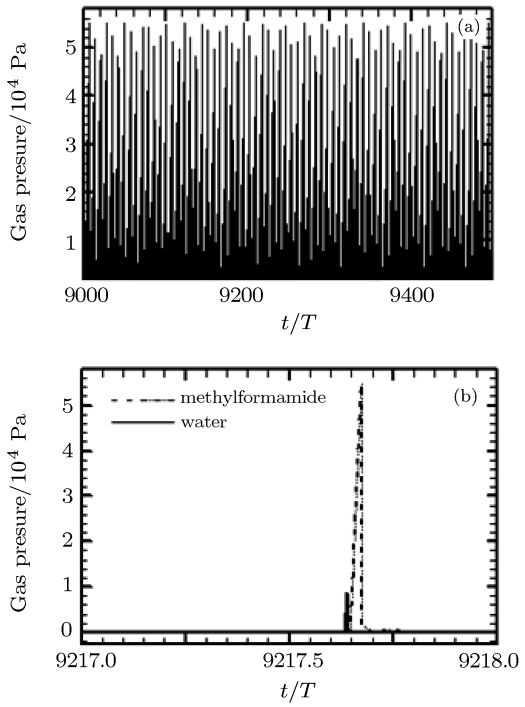


Fig. 6. (a) Variations of the gas pressure for the gas-filled bubble in N-methylformamide with time. The calculation is performed for the maximum pressure, for which the bubble parameters are maximized. $R_0 = 8$ μm, $P_a = 1.56$ atm. (b) A comparison between the maximum values of the gas pressure in water and in N-methylformamide.

From Figs. 6 and 7, we can see that the bubble temperature and the interior gas pressure in N-methylformamide are much higher than those in water and as a consequence, the light intensity produced by the bubble in Methylformamide is higher than that in water, as shown in Fig. 8. It can be demonstrated that as the bubble interior temperature increases, the light intensity increases.

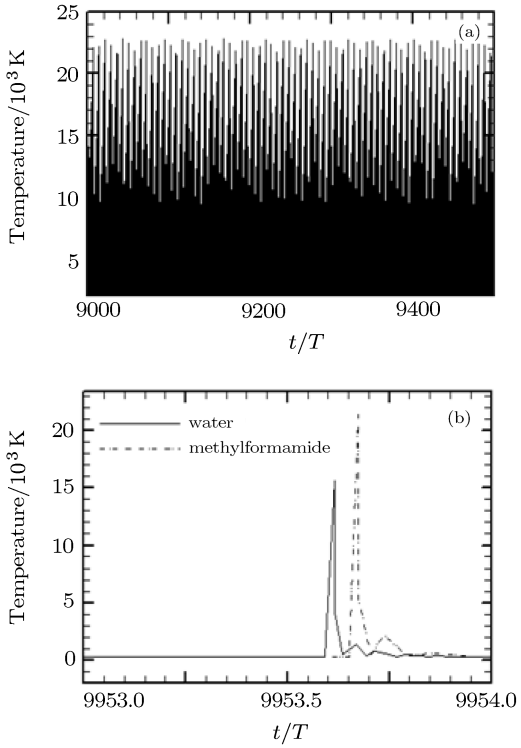


Fig. 7. (a) The variation of the interior temperature versus time with the maximum pressure for the N-methylformamide. (b) A comparison between the maximum values of temperature in water and in N-methylformamide.

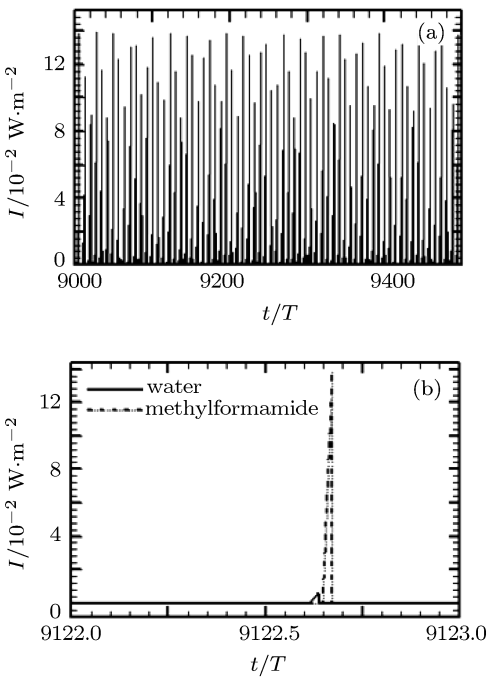


Fig. 8. (a) Light intensity for the selected pressure value in N-methylformamide. $R_0 = 8$ μm, $P_a = 1.56$ atm. (b) A comparison between the maximum values of light intensity in N-methylformamide and in water.

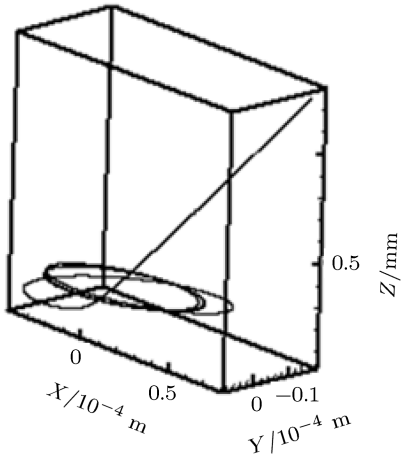


Fig. 9. Bubble trajectory numerically drawn for the initial parameters $R_0 = 8$ μm, $P_a = 1.56$ atm, showing the elliptic path clearly.

Figure 9 shows the elliptic path of the moving-SBSL in N-methylformamide. In comparison with the trajectory in water, which is shown in Fig. 2, it can be seen that as the fluid viscosity increases, the bubble trajectory shape changes from circular to elliptic and the diameter of the bubble trajectory turns larger correspondingly. This increase of the trajectory diameter is due to an increase in the maxima of all components of the hydrodynamics force, which result in the exertion of an additional momentum from the fluid on the sonoluminescing bubble.

4. Conclusion

The unique circular path of a moving single bubble sonoluminescence in water is identified for the first time. It is shown that there is a maximum pressure for the m-SBSL in water, with which all bubble parameters are maximized. It is found that as the ambient pressure increases, the light intensity increases correspondingly. The obtained bubble parameters for the water case are compared with those for the N-methylformamide case with the same initial condition. It is also found that the light intensity is directly related to the bubble interior temperature. It is observed that as the fluid viscosity increases, the light intensity increases, which is in good accordance with the earlier experimental results reported by Didenko *et al.* in 2000.

References

[1] Arakari V H 2003 *Curent Science* **85** 7
[2] Moss W C, Clarke D B and Young D A 1997 *Science* **276** 1398
[3] Wu C C and Roberts P H 1993 *Phys. Rev. Lett.* **70** 3424
[4] Moss W C, Clarke D B, White J W and Young D A 1994 *Phys. Fluids* **6** 2979
[5] Yasui K 1999 *Phys. Rev.* E **60** 1754
[6] Vuong V Q, Szeri A S and Young D A 1999 *Phys. Fluids* **11** 10
[7] Didenko Y T, McNamara W B and Suslick K 2000 *Nature* **407** 877
[8] Vazquez G E and Putterman S J 2000 *Phys. Rev. Lett.* **85** 14
[9] An Y 2006 *Phys. Rev.* E **74** 026304
[10] An Y and Ying C F 2005 *Phys. Rev.* E **71** 036308
[11] Xu J, Chen W, Xu X, Liang Y, Huang W and Gao X 2007 *Phys. Rev.* E **76** 026308
[12] Magnaudet J and Legendre D 1998 *Phys. Fluids* **10** 550
[13] Toegel R, Lutter S and Lohse D 2006 *Phys. Rev. Lett.* **96** 114301
[14] Yasui K 1997 *Phys. Rev.* F **56** 6750
[15] Lofstedt R, Barber B P and Putterman S J 1993 *Phys. Fluids* A **5** 2911
[16] Barber B P, Hiller R, Lofstedt R and Putterman S J 1997 *Phys. Rep.* **281** 65
[17] Sadighi-Bonabi R, Rezaei-Nasirabad R and Galavani Z 2009 *J. Acoust. Soc. Am.* **126** 2266
[18] Loftstedt R, Weninger K, Putterman S and Barber B R 1995 *Phys. Rev.* E **51** 4400
[19] Hilgenfeldt S, Grossman S and Lohse D 1999 *Phys. Fluids* **11** 1318
[20] Taylor R L and Caledonia G 1969 *J. Quant. Spectrosc. Radiat. Transf.* **9** 657
[21] Ketterling J A and Apfel R E 2000 *J. Acoust. Soc. Am.* **107** 819
[22] Troia A, Ripa D M and Spagnolo R 2006 *Ultrason.* **13** 278
[23] Lide D R (editor) 2005 *CRC Handbook of Chemistry and Physics* (Boca Raton: CRC Press) pp. 256–300